AGU100 ADVANCING EARTH AND SPACE SCIENCE

Geophysical Research Letters

RESEARCH LETTER

10.1029/2018GL080742

Key Points:
- Abrupt V_P/V_S changes occurred in the upper crust of the Japanese islands after the 2011 Tohoku-Oki megathrust earthquake
- Peak V_P/V_S changes developed along the paths subparallel or subperpendicular to the megathrust
- Azimuthal seismic anisotropy developed due to the lithospheric displacements caused by the megathrust earthquake

Supporting Information:
- Supporting Information S1
- Supporting Information S2
- Data Set S1
- Data Set S2
- Data Set S3

Correspondence to:
T.-K. Hong,
tkhong@yonsei.ac.kr

Citation:
Kim, I., & Hong, T.-K. (2018). Azimuthal seismic anisotropy in the upper crust of the Japanese islands induced by the 2011 Tohoku-Oki megathrust earthquake. *Geophysical Research Letters*, *45*, 12,793–12,803. https://doi.org/10.1029/2018GL080742

Received 2 OCT 2018
Accepted 26 NOV 2018
Accepted article online 28 NOV 2018
Published online 11 DEC 2018

Azimuthal Seismic Anisotropy in the Upper Crust of the Japanese Islands Induced by the 2011 Tohoku-Oki Megathrust Earthquake

Ilgoo Kim[1] and Tae-Kyung Hong[1]

[1]Department of Earth System Sciences, Yonsei University, Seoul, South Korea

Abstract We investigated V_P/V_S changes in the upper crust of the Japanese islands after the 2011 M_W9.0 Tohoku-Oki megathrust earthquake. Abrupt V_P/V_S changes with azimuth-dependent variations were observed after the megathrust earthquake. The V_P/V_S changes ranged between −0.0458 (±0.0012) and 0.0422 (±0.0033). Large localized V_P/V_S changes over regional distances suggested medium-dependent deformation. Peak V_P/V_S changes were observed along paths subparallel or subperpendicular to the directions toward the megathrust earthquake. The V_P/V_S changes displayed characteristic 2θ variations as a function of the azimuth difference, suggesting azimuthal seismic anisotropy. The V_P/V_S ratio recovered gradually over time. Some regions presented permanent V_P/V_S changes. The azimuthal seismic anisotropy may have developed from preferential crack orientation as a consequence of the combined effects of lithospheric displacements and a depth-dependent ambient stress field. It appears that recovery of the medium properties may take decades.

Plain Language Summary We report a unique observation of azimuthal seismic anisotropy in the upper crust of Japanese islands, which was induced by the 2011 *M*9.0 Tohoku-Oki megathrust earthquake. The azimuthal seismic anisotropy was caused by the direction-dependent discriminative lithospheric displacement during the megathrust earthquake. We analyzed the traveltimes of local seismic waves and estimated the changes in V_p/V_s ratios after the megathrust earthquake. We observed the abrupt V_p/V_s changes after the megathrust earthquake. The V_p/V_s ratios recovered gradually with time for several years. This study may provide important information on the medium property changes after the megathrust earthquake and will be useful for mitigation of potential seismic hazards.

1. Introduction

The 11 March 2011 M_W9.0 Tohoku-Oki earthquake occurred on the convergent margin between the Pacific plate and the Okhotsk plate. The megathrust earthquake produced lithospheric coseismic and postseismic viscoelastic deformations over local and regional distances (Hong et al., 2015; Lee & Hong, 2014; Sun et al., 2014; Yamagiwa et al., 2015). Field observations showed that the coseismic lateral displacements reached ~1.8 m on the west coast of the Japanese islands near the epicenter, ~5.6 m on the nearest east coast of the Japanese islands, and ~31.1 m on the ocean floor near the epicenter (Kido et al., 2011; S. Ozawa et al., 2011; Silverii et al., 2014; Simons et al., 2011; Sun et al., 2014). The volcanic regions of the Japanese islands presented coseismic surface subsidence of 5–15 cm over a horizontal distance of 15–20 km (T. Ozawa & Fujita, 2013; Takada & Fukushima, 2013). The 1-year postseismic displacements reached ~0.5 m on the west coast near the epicenter, ~0.7 m on the nearest east coast, and ~0.5 m on the ocean floor near the epicenter (Sun et al., 2014). Additional description on the properties of the megathrust earthquake is presented in the supporting information (Asano et al., 2011; Hirose et al., 2011; Hoshiba et al., 2011; Irikura & Kurahashi, 2012; Lay et al., 2011; Matsumoto et al., 2010; Peng et al., 2012; Shao et al., 2011; Tormann et al., 2015; Yagi & Fukahata, 2011; Yukutake et al., 2011).

The megathrust earthquake produced strong seismic waves and large lithospheric displacements at regional distances (Hong et al., 2015; Lee & Hong, 2014; S. Ozawa et al., 2011; Sun et al., 2014, Yamagiwa et al., 2015). Strong seismic waves accompanied large dynamic stress changes, which were particularly apparent in volcanic regions with incorporated surface subsidence and seismic velocity reduction (Brenguier et al., 2014;

10.1029/2018GL080742

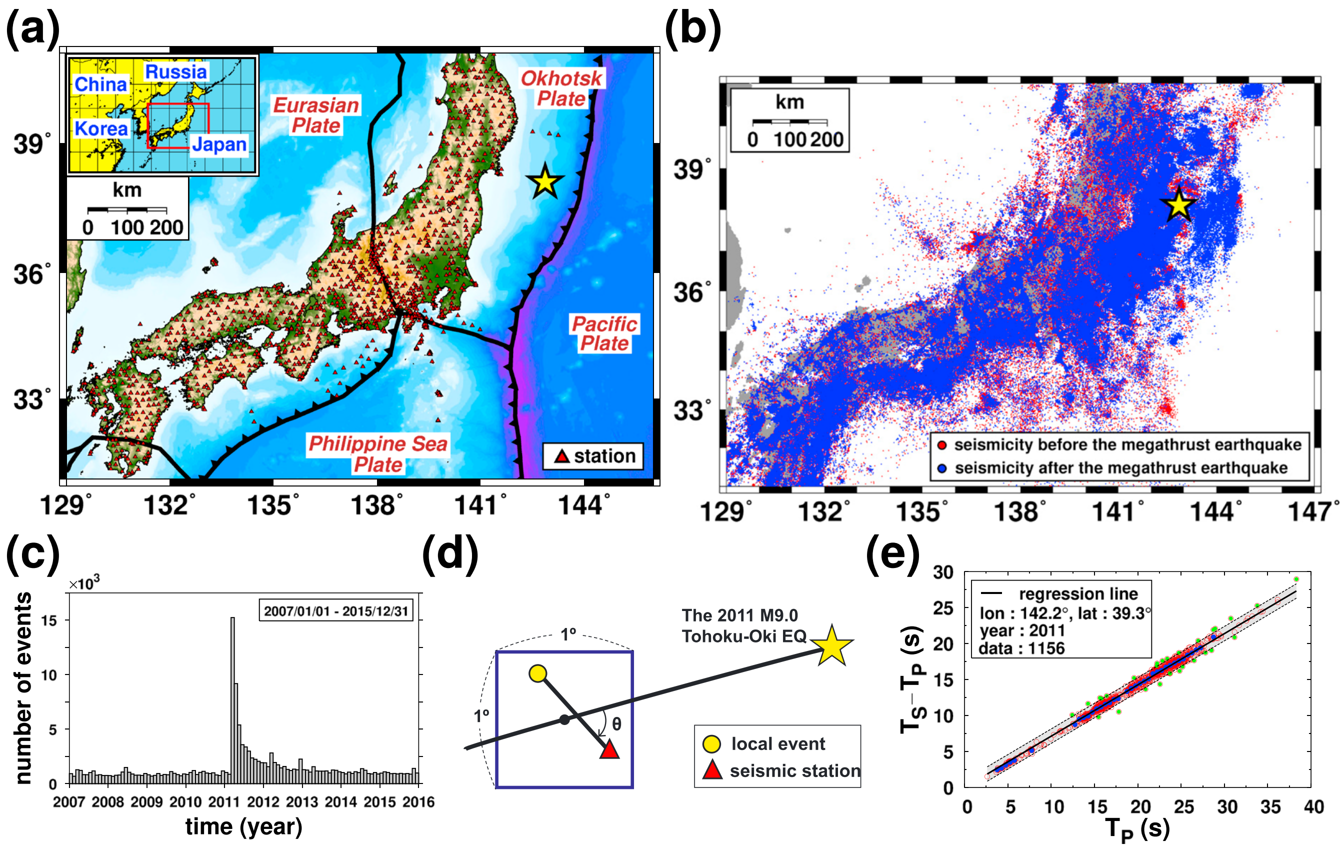

Figure 1. (a) Map of stations (triangles) and tectonic environment. The epicenter of the 2011 Tohoku-Oki megathrust earthquake is marked with a filled star. (b) Map of events from 2007 to 2015. The seismicity before and after the megathrust earthquake is presented. (c) Histogram showing the numbers of earthquakes with magnitude greater than or equal to 2.6 that is the minimum magnitude ensuring the completeness of the earthquake catalog (A. Cao & Gao, 2002; Wiemer & Wyss, 2000). The number of events increased after the megathrust earthquake. (d) Schematic showing the raypath and the direction toward the megathrust earthquake along the great circle. The azimuth difference (θ) of the raypath is measured clockwise with respect to the direction from the center of a cell to the megathrust earthquake (star) along the great circle. The station (triangle) and the local event (circle) are marked. (e) Determination of the V_P/V_S ratio using a modified Wadati diagram. Outliers are marked with open circles.

Takada & Fukushima, 2013). Lithospheric displacements caused by the megathrust earthquake perturbed the regional crust, incorporating static stress field changes (Hong et al., 2015; Porritt & Yoshioka, 2017). The perturbations of the medium were particularly strong in thermally weakened regions (Takada & Fukushima, 2013). Additionally, these perturbations incorporated changes in seismicity (Shimojo et al., 2014; Terakawa et al., 2013).

Seismic velocity changes have been observed widely in the shallow subsurface after strong earthquakes (Chaves & Schwartz, 2016; Taira et al., 2015; Xu & Song, 2009). The decrease in seismic velocity reached 50% in the Japanese islands after the Tohoku-Oki megathrust earthquake (Nakahara, 2015; Nakata & Snieder, 2011; Sawazaki & Snieder, 2013; Takagi & Okada, 2012). It was reported that the seismic velocity and medium strength recovered over time after strong earthquakes with magnitudes greater than M_W6.0, following a power law (e.g., Baisch & Bokelmann, 2001; Brantut, 2015; Brenguier et al., 2008; Chaves & Schwartz, 2016; Hong et al., 2017; Ikuta et al., 2002; Nakata & Snieder, 2011; Schubnel et al., 2005; Vidale & Li, 2003).

Changes in the seismic velocity have only been resolved in the shallow subsurface through analyses of vertically incident shear waves and ambient noise (or coda; Brenguier et al., 2014; Minato et al., 2012; Nakahara, 2015; Nakata & Snieder, 2011; Sawazaki & Snieder, 2013; Takagi & Okada, 2012). However, studies have analyzed fundamental mode Rayleigh waves to determine the change in the seismic velocity in the lower crust of the Korean Peninsula after the megathrust earthquake (Hong et al., 2015, 2017). The lower crustal velocity changes presented characteristic azimuthal variations that might have been caused by a directional perturbation of the medium (Hong et al., 2017).

Investigation of medium perturbation was limitedly made to shallow subsurface and lower crust. Medium perturbation of the upper crust caused by megathrust earthquake is poorly understood. Therefore, we investigate changes in medium properties in the upper crust of the Japanese islands after the Tohoku-Oki megathrust earthquake using an analysis of local seismic waves in terms of the Poisson's ratios that can be inferred from the V_P/V_S ratios. In addition, we investigate the crustal response and stress perturbation related to the megathrust earthquake.

2. Data and Methods

We analyze the earthquakes with focal depths less than 25 km around the Japanese islands in 2007–2015. We constrain the focal depths to study the properties of the upper crust. We collected event and station information, including the event locations and origin times, station locations, and phase arrival times from the Japan Meteorological Agency. The number of events is approximately 1.2 million (Figure 1). The event magnitudes are greater than −1.4. Dense seismic stations are deployed on the Japanese islands. The number of stations is 1,349, composing the spatial distribution of stations with an average interstation distance of ∼10 km.

We analyze the traveltimes of the seismic phases in the upper crust events. The V_P/V_S ratio is estimated using a modified Wadati method based on the P and S traveltimes (Jo & Hong, 2013; Nur, 1972; Wadati, 1933):

$$\frac{V_P}{V_S} = \frac{T_S - T_P}{T_P} + 1, \tag{1}$$

where T_P is the P traveltime and T_S is the S traveltime. A representative V_P/V_S ratio is found using a least squares fitting method with uniform weights on discrete T_P windows.

Spatiotemporal clustering of earthquakes may yield incorrect estimates in V_P/V_S measurement since the data sets for the clustered events represent the properties of the localized areas (Lees & Crosson, 1989). The influence of spatiotemporal seismicity changes can be minimized by analyzing data points that are distributed uniformly with traveltime (e.g., Lees & Crosson, 1989). We determine representative traveltime values for discrete traveltime bins (see the supporting information). Outliers with deviations greater than 1 s from the linear regression line are removed from the data set to enhance the stability of the analysis. The linear regression line is refined based on the data set with outliers excluded (Jo & Hong, 2013). The refinement process is repeated until the changes in the regression lines are smaller than the prescribed value (Figure 1).

The V_P/V_S ratios are estimated using the traveltimes of the P and S waves that are transmitted through the medium discretized by cells with an uniform size of 1°-by-1°. The V_P/V_S ratio is calculated for every 0.2° of latitude and longitude (see the supporting information). Each cell is overlapped with adjacent cells by 0.8° in longitude and latitude. The interval between the centers of adjacent cells is 0.2°. The yearly V_P/V_S ratios are calculated from 2007 to 2015. The stability of the results is examined using a bootstrap analysis (Efron & Tibshirani, 1991; Hong & Menke, 2008; Jo & Hong, 2013; Revenaugh & Meyer, 1997; see the supporting information). We generate 100 resampled traveltime data sets with an allowance for multiple selections. The V_P/V_S ratios are determined based on the 100 data sets. The average V_P/V_S ratios and the standard errors are estimated. The 95% confidence intervals of the V_P/V_S estimates are determined using the standard errors (see the supporting information).

We measure the azimuth differences between the raypaths of the seismic phases of local earthquakes and the direction toward the megathrust earthquake along the great circle. The azimuth differences vary between −90° and 90°. The azimuth differences are divided into 12 azimuthal ranges, each with a bandwidth of 15° (Figure 1). The V_P/V_S ratios are based on a traveltime data set that is classified into the 12 azimuth ranges. We determine the V_P/V_S ratios of the discretized media with cell-hit-counts of 60 or greater (see the supporting information). The cell-hit-counts are larger than 60 in most regions, which is sufficiently high for stable estimation of V_P/V_S ratios.

The average V_P/V_S ratios of discretized media are calculated for discrete azimuth ranges with a uniform band width of 15° using data sets in 30-day-long windows, shifting by 10 days with 20 days of overlap between adjacent windows. The V_P/V_S ratios may vary with the effective stress and medium properties (Brantut, 2015; Schubnel et al., 2005). The temporal recovery of medium properties (V_P/V_S ratio) may be represented with an exponential function (Hong et al., 2017; Keulen et al., 2008; Nakata & Snieder, 2011; Vidale & Li, 2003):

$$\Delta\left[\frac{V_P}{V_S}\right]_t = \left[\frac{V_P}{V_S}\right]_t - \left[\frac{V_P}{V_S}\right]_0 = a\exp(-bt), \tag{2}$$

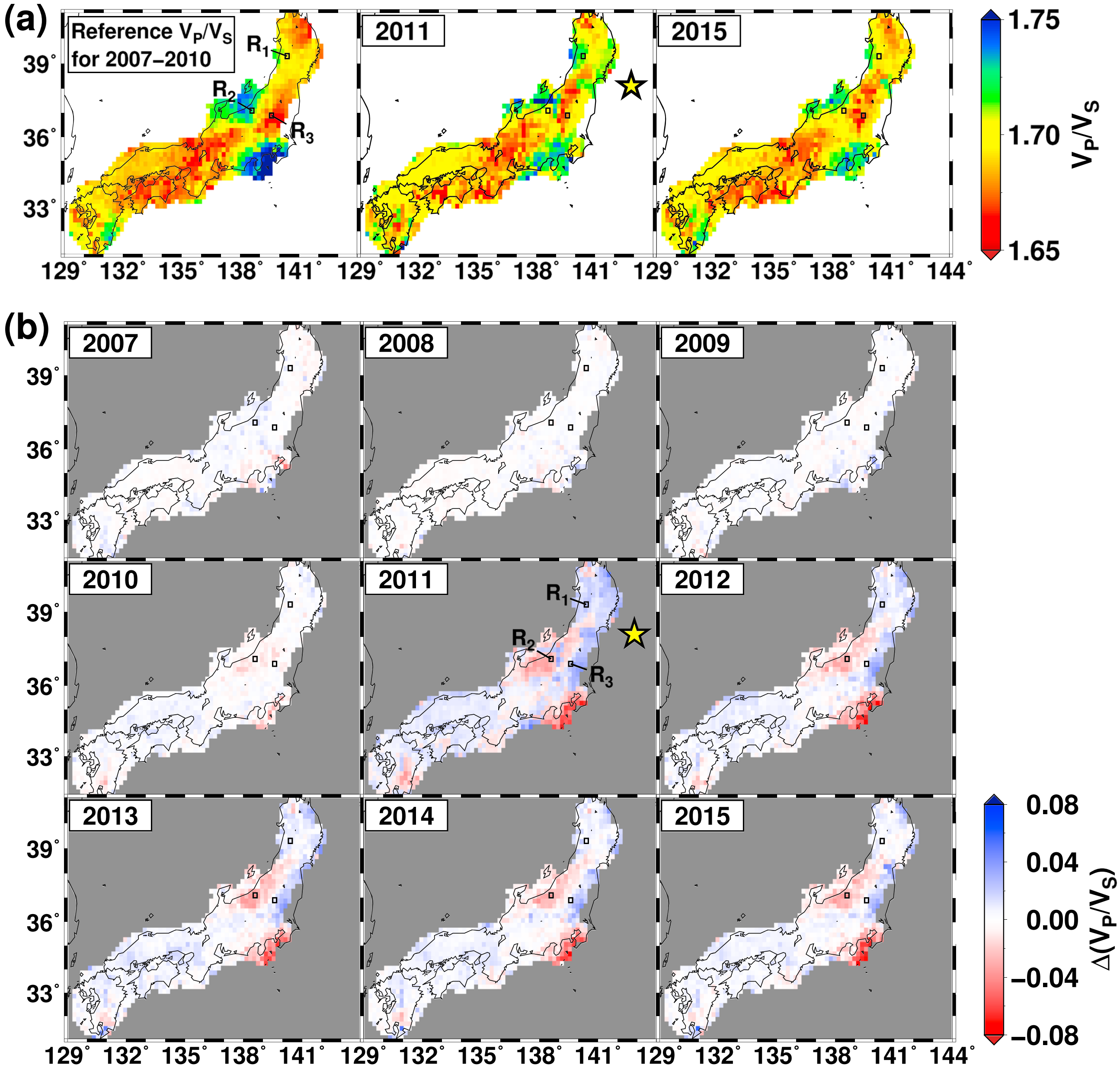

Figure 2. (a) Reference V_P/V_S ratios for 2007–2010 and annual V_P/V_S ratios for 2011 and 2015. (b) Peak V_P/V_S change in the upper crust of the Japanese islands from 2007 to 2015. Abrupt V_P/V_S changes are observed after the 2011 M_W9.0 Tohoku-Oki megathrust earthquake (star). The magnitude of the change in V_P/V_S decreases over time. Three representative locations (R_1, R_2, and R_3) are marked. The V_P/V_S ratios changed abruptly after the megathrust earthquake.

where t is the time lapse in days after the medium perturbation, $\Delta\left[\frac{V_P}{V_S}\right]_t$ is the difference between V_P/V_S for time lapse t ($\left[\frac{V_P}{V_S}\right]_t$) and the reference value of V_P/V_S before the medium is perturbed ($\left[\frac{V_P}{V_S}\right]_0$), a is the instantaneous change in V_P/V_S, and b is the recovery rate per day. The best fit constants a and b are determined using a grid search (see the supporting information). Uncertainty ranges of a and b at the 95% confidence level are estimated from the data fitting to the theoretical exponential curve. Additional discussion on the analysis can be found in the supporting information (S. Cao & Greenhalgh, 1995; Carpenter & Cash, 1988; Gonzalez-Huizar et al., 2012; Houng et al., 2016).

3. Upper Crustal V_P/V_S Changes

We calculate the annual V_P/V_S ratios for 2007 to 2015. The reference V_P/V_S ratios are calculated based on the data set of January 2007 to August 2010, which is before the megathrust earthquake. We measure the

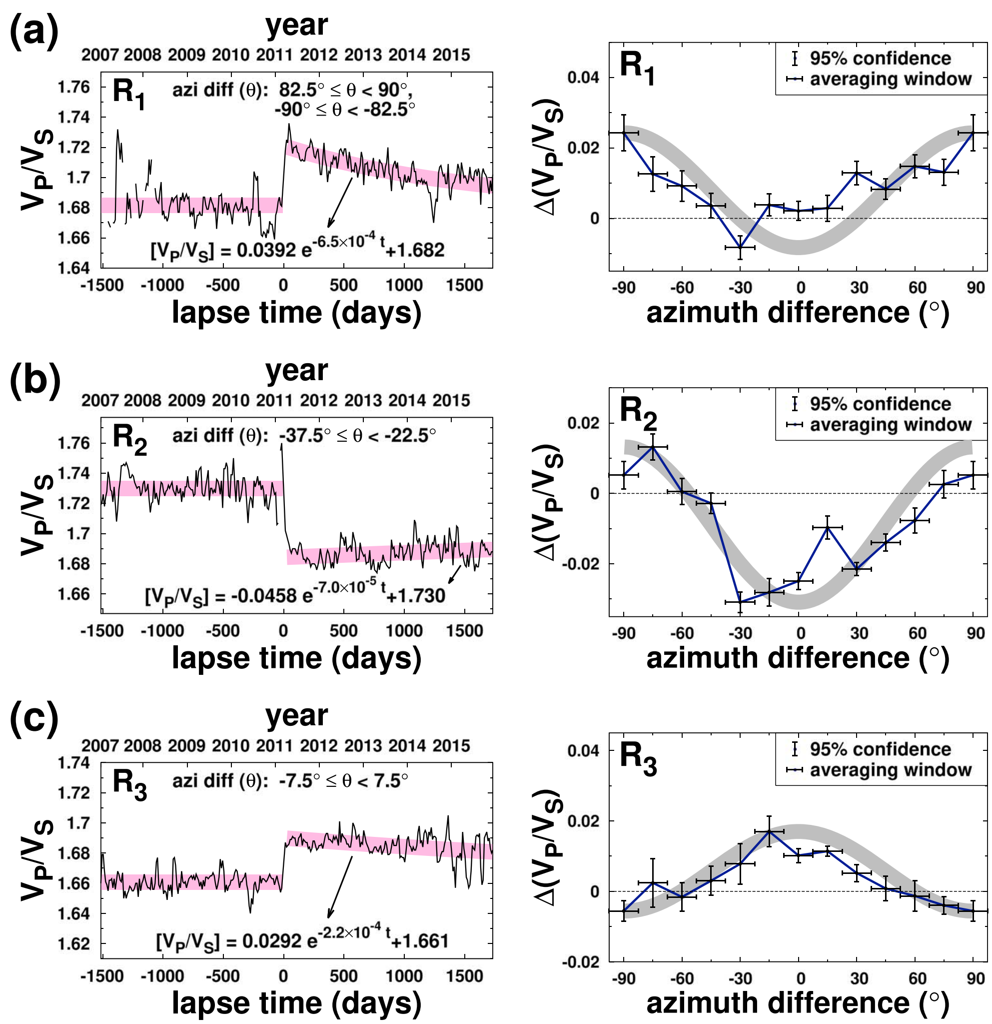

Figure 3. Temporal changes in the V_P/V_S variations after the megathrust earthquake (left column) and azimuthal variations in the instantaneous V_P/V_S variations (right column) for regions (a) R_1, (b) R_2, and (c) R_3. The temporal changes in the V_P/V_S variations are presented for given azimuth differences (θ). The temporal and azimuthal variations of the V_P/V_S ratio are fitted with theoretical exponential curves (thick solid lines). The functions for the fitted lines are noted. The V_P/V_S ratio changes abruptly after the megathrust earthquake and recovers gradually over time. The V_P/V_S changes display characteristic 2θ azimuthal variations. The 95% confidence intervals of the V_P/V_S changes as a function of the azimuth differences are marked with bars.

differences between the annual V_P/V_S ratios and reference V_P/V_S ratios. We observe apparent changes in the V_P/V_S ratios over the Japanese islands after the megathrust earthquake (Figure 2). The observed instantaneous V_P/V_S changes right after the megathrust earthquake range between −0.0848 (±0.0153) and 0.0496 (±0.0108; Figure 2). We observe a rapid recovery of V_P/V_S ratios with time, which can be fitted with an exponential curve in (2) (Figure 3).

The temporal V_P/V_S recovery follows an exponential curve in equation (2). The observed V_P/V_S changes are fitted with the theoretical curve. The peak V_P/V_S changes (a) vary between −0.0458 (±0.0012 at the 95% confidence level) and 0.0422 (±0.0033). The uncertainties of constants a and b are assessed using the likelihood functions based on the standard deviations of errors (Bevington & Robinson, 2003).

We find distinct V_P/V_S changes in the central Japanese islands (Honshu; Figure 2). The west central Honshu region exhibits large decreases in V_P/V_S, whereas the east central and northern Honshu regions exhibit large increases in V_P/V_S ratios. In general, the V_P/V_S changes are positive in the regions of low V_P/V_S ratios (less than 1.69) and negative in the regions of high V_P/V_S ratios (higher than 1.69; Figure 2).

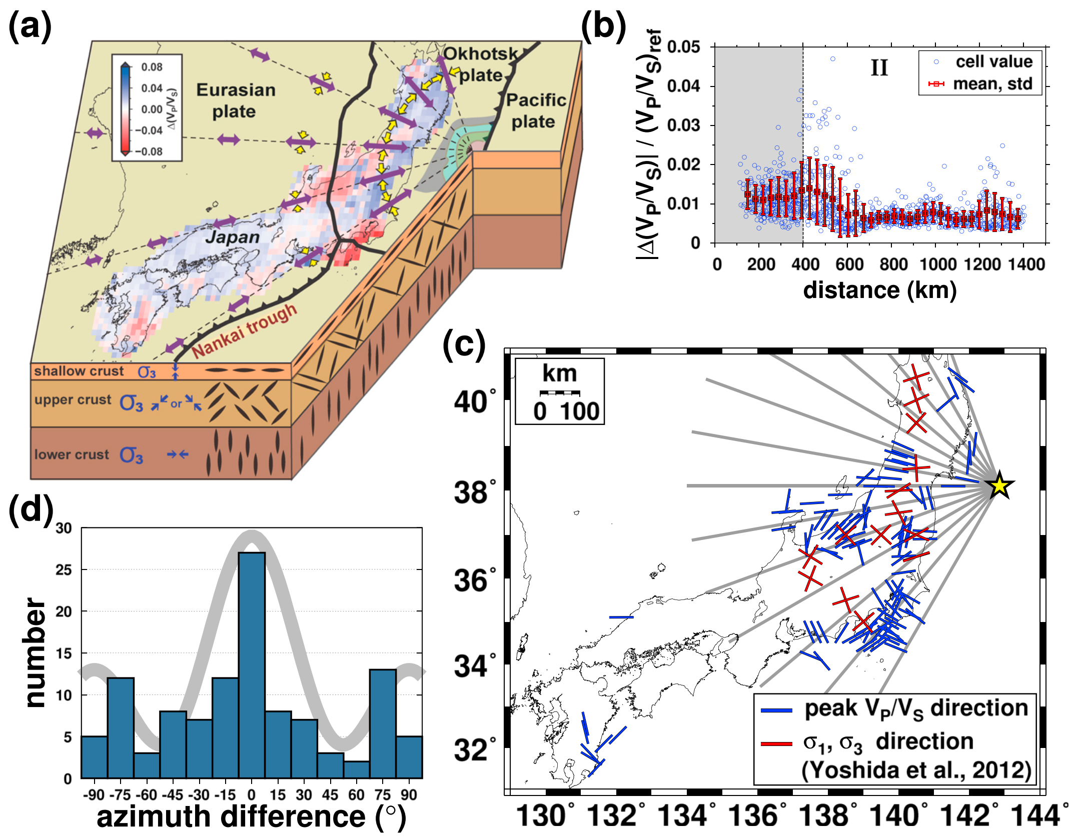

Figure 4. Medium perturbation due to the megathrust earthquake. (a) A schematic model of the crack orientation with increasing depth for the lateral lithospheric displacements. The orientation of the minimum stress component rotates with depth along the vertical axis due to the vertical loading of overburden layers. The crack orientation produces characteristic azimuthal seismic anisotropy. (b) Distance-dependent variation of the peak changes in V_P/V_S. The average values of the discrete distance bins with a size of 70 km are presented. Discrete distance bins are shifted by 35 km. The V_P/V_S changes decrease with distance in regions at distances greater than 400 km. (c) Orientation of the peak V_P/V_S changes and principal stresses after the megathrust earthquake. The orientations of peak V_P/V_S changes (blue bars) and maximum and minimum stress components (red bars, Yoshida et al., 2012) are indicated. (d) Histogram for the orientations of peak V_P/V_S changes. The histogram presents a bimodal distribution, suggesting the peak V_P/V_S changes in directions subparallel or subperpendicular to the megathrust earthquake.

We examine the stability of the V_P/V_S ratios using a bootstrap analysis with 100 resampled data sets. The V_P/V_S ratios are estimated for the resampled data sets. The standard errors of the V_P/V_S estimates from the bootstrap analysis are less than 0.005 in most inland regions with at least 60 data points, which suggest stable results (see the supporting information).

The V_P/V_S ratios recover over time. The temporal changes in the V_P/V_S ratios are consistent with the theoretical variation following an exponential curve (Figure 3). The magnitudes of the V_P/V_S changes are, in general, inversely proportional to the distances from the megathrust earthquake (Figure 4). The lateral distribution of the V_P/V_S changes is observed consistently for more than 4 years. Additionally, we find that the V_P/V_S change varies with the azimuth in the direction toward the megathrust earthquake along the great circle (supporting information; Figure 3).

We select three representative regions for comparison of temporal V_P/V_S ratios (R_1, R_2, and R_3 in Figure 2). The instantaneous change in V_P/V_S (a) reached 0.0392 ($\pm$0.0019) in region R_1, -0.0458 ($\pm$0.0012) in region R_2, and 0.0292 ($\pm$0.0014) in region R_3 for various azimuth differences θ. The recovery rate (b) reached 0.0014 ($\pm$0.0004) day^{-1} in region R_1, 0.0011 ($\pm$0.0002) day^{-1} in region R_2, and 0.0003 ($\pm$0.00005) day^{-1} in region R_3 (Figure 3). The Poisson's ratio changes equivalent to the instantaneous V_P/V_S changes range from -0.0213 ($\pm$0.0006) to 0.0204 ($\pm$0.0016).

The recovery rate of the V_P/V_S ratio appears to vary by region. It took 23 months in region R_1 for the temporal V_P/V_S ratios to reach the 95% confidence interval of the reference V_P/V_S ratios before the megathrust earthquake. The V_P/V_S ratios recovered by ~13% in region R_2 and ~44% in region R_3 after 4 years. Full recovery of V_P/V_S ratios may take 461 months (38.4 years) in region R_2 and 131 months (10.9 years) in region R_3, according to the theoretical curves.

The V_P/V_S changes are high on the paths subparallel or subperpendicular to direction toward the megathrust earthquake along the great circle, which is very apparent far from the megathrust earthquake. (Figure 4). This may be because the medium's deformation is very complex at short distances due to the influence of the rupture dimension. The V_P/V_S changes may result from physical perturbation of the medium (Miyazawa, 2011). The positive and negative changes in V_P/V_S may be associated with changes in the crack density and rock properties (Crampin & Chastin, 2003; Fortin et al., 2007; Shearer, 1988; Wang et al., 2012).

4. Seismic Anisotropy

We observe angular periodicity of π (2θ variation) as a function of the azimuth difference θ in the V_P/V_S changes (Figure 3). No azimuthal seismic anisotropy was apparent before the megathrust earthquake (see the supporting information). This observation suggests that seismic anisotropy may be associated with the perturbation of the medium by the coseismic and postseismic lithospheric displacements.

The cracks produced by the lithospheric displacements may be responsible for both the V_P/V_S changes and the seismic anisotropy (Crampin & Chastin, 2003; Shearer, 1988). The differential stress increase due to lithospheric displacement results in cracks aligned along the maximum stress orientation. The aspect ratio of such cracks increases with the differential stress (Crampin & Zatsepin, 1995; Zatsepin & Crampin, 1997).

A pressure change in the high-pressure regime greater than 200 MPa (equivalently, a depth of 7.4 km below the surface; Brown & Hoek, 1978; Brudy et al., 1997; Haimson & Chang, 2002) rarely causes a change in the V_P/V_S ratios (Christensen, 1996). On the other hand, the V_P/V_S ratios may change significantly with a pressure change in the low-pressure regime of approximately 40 MPa or less (equivalently, a depth of 1.5 km; Nakahara, 2015; Nakata & Snieder, 2011; Sawazaki & Snieder, 2013; Takagi & Okada, 2012). The V_P/V_S ratios in the upper crustal regions appear to respond pressure changes.

The V_P/V_S ratio of wet rock increases with decreasing pressure, whereas that of dry rock decreases with decreasing pressure (Wang et al., 2012). The aspect ratio of cracks is another factor that controls the V_P/V_S ratio. The V_P/V_S ratio of wet rock decreases as the aspect ratio increases for a given crack density (Fortin et al., 2007; Wang et al., 2012). Additionally, the V_P/V_S ratio of wet rock generally increases with the crack density, whereas that of dry rock decreases with the crack density (Fortin et al., 2007; Wang et al., 2012).

The V_P/V_S ratio may vary with the crack orientation with respect to the direction of wave incidence, producing seismic anisotropy (Anderson et al., 1974; Shearer, 1988). The distance-dependent lithospheric displacements due to the megathrust earthquake may decrease the effective stress in the medium, thereby increasing the crack density. The vertical stress component induced by loading in the overburden layer generally increases with depth. Therefore, the minimum stress component is oriented vertically near the surface and rotates with increasing depth (Crampin, 1990; Lee et al., 2017). This unique ambient stress field develop cracks in depth-dependent orientations (Figure 4).

Horizontally oriented cracks in the shallow crust may be responsible for the apparent decrease in the seismic velocity of vertically traveling seismic waves (e.g., Lockner et al., 1977; Shearer, 1988). The vertical rotation of the minimum stress orientation may lead to vertically slanted cracks in the upper crust (Figure 4). Cracks in the lower crust and upper mantle may be aligned subparallel or subperpendicular to the direction of the megathrust earthquake along the great circle, which can be resolved from an analysis of low-frequency surface waves (Hong et al., 2015). However, the orientations of the greatest V_P/V_S changes are complex at short distances from the megathrust earthquake due to the complex medium deformation (Figure 4b).

5. Discussion and Conclusions

We investigated the azimuthally anisotropic V_P/V_S changes in the upper crust of the Japanese islands induced by the 2011 Tohoku-Oki megathrust earthquake. The V_P/V_S changes varied between −0.0458 (±0.0012) and 0.0422 (±0.0033), displaying 2θ azimuthal anisotropy. The V_P/V_S changes were positive in the regions of low V_P/V_S ratios and negative in the regions of high V_P/V_S ratios (Figure 2). The low V_P/V_S regions are placed around the volcanic front where the media are perturbed by fluid-filled cracks that are distributed in the upper crust (Kaneshima et al., 1988; Nakajima et al., 2001; Okada et al., 2015). The release of stress stored in the media might induce crack alignment, which causes azimuth-dependent V_P/V_S changes.

The Poisson's ratio changes corresponding to the V_P/V_S changes range −8.55% (±0.25% in the 95% confidence interval) to 9.08% (±0.71% in the 95% confidence interval). These Poisson's ratio changes suggest that perturbations of the medium were larger in the upper crust of the Japanese islands than they were in the lower crust of the Korean Peninsula. The medium perturbations in the crusts of the Japanese islands and the Korean Peninsula suggest regional-scale crustal deformation due to the 2011 Tohoku-Oki megathrust earthquake.

The temporal recovery rate (*b*) varies with distance and depth. The recovery rate of the shear wave velocity (*b*) was found to range from 0.0013 (±0.0002 at the 95% confidence level) day^{-1} to 0.0157 (±0.0063 at the 95% confidence level) day^{-1} in the lower crust of the Korean Peninsula (Hong et al., 2017). These recovery rates are larger than those observed in the upper crust of the Japanese islands. The upper crust of the Japanese islands takes longer to recover its medium properties than the lower crust of the Korean Peninsula does, which may be due to the proximity of the Japanese islands to the megathrust earthquake. The distance- and depth-dependent characteristics may be associated with characteristic medium perturbations due to the megathrust earthquake (Brantut, 2015; Schubnel et al., 2005).

It is intriguing to note that the magnitudes of the V_P/V_S changes are comparable at distances of less than ∼400 km from the megathrust earthquake (regime I in Figure 4c). This may be because the medium deformation may be complex at short distances, preventing uniaxial deformation, which prevails at large distances (Hong et al., 2017). However, the V_P/V_S changes generally decreased with distance at large distances (> ∼400 km).

The lithospheric displacements caused by the 2011 Tohoku-Oki megathrust earthquake caused discriminative spatially inhomogeneous medium perturbations. The lithospheric deformation may have formed cracks aligned with the maximum stress component (σ_1) and closed cracks oriented along the minimum stress component (σ_3) (Crampin & Chastin, 2003). It is known that the V_P/V_S ratio generally increases with the differential stress ($\sigma_1 - \sigma_3$) (Shearer, 1988; Yoshida et al., 2012). The V_P/V_S changes may be enhanced by the differential stress changes associated with the lithospheric displacements. Increased seismicity in unprecedented fault types and orientations were observed in the regions of V_P/V_S changes (Hasegawa et al., 2012; Imanishi et al., 2012; Kato et al., 2011; Lee & Hong, 2014; Yoshida et al., 2012).

This study suggests that the direction-dependent lithospheric displacement and the spatially inhomogeneous dynamic response of the medium produce seismic anisotropy (Nakata & Snieder, 2012; Zatsepin & Crampin, 1997; Figure 4a). The release of crustal stress by lithospheric displacements might be associated with the medium perturbation.

The orientations of peak V_P/V_S changes are consistent with those of compression axis and tension axis in the crust after the megathrust earthquake (Yoshida et al., 2012; Figure 4b). Also, the orientations of peak V_P/V_S changes agree with the fast polarization directions in the upper crust of local regions such as the central Honshu (Iidaka et al., 2014; Iidaka & Obara, 2013; Ikeda & Tsuji, 2014). It is intriguing to note that the azimuthal seismic anisotropy in V_P/V_S changes is consistent with the apparent shear wave splitting feature in the shallow crust (Nakata & Snieder, 2012). However, we find little correlation between the V_P/V_S changes in the upper crust and the seismic velocity changes in the shallow crust (Brenguier et al., 2014; Minato et al., 2012; Nakahara, 2015; Nakata & Snieder, 2011; Takagi & Okada, 2012), which may be due to discriminative depth-dependent medium deformation.

The V_P/V_S changes in the lower crust are little according to an analysis of local traveltime data (see the supporting information). This may be because the geometrical shapes of medium perturbation induced by the megathrust earthquake are different between the upper and lower crusts (Ikeda & Tsuji, 2014). The characteristic orientations of medium perturbations (e.g., cracks) in the upper crust may be effectively resolved by local seismic waves that naturally have vertical incidence angles around 70° (Wang et al., 2012). It is intriguing to note that the induced seismic anisotropy in the lower crust of the Japanese islands is generally consistent with that in the lower crust of the Korean Peninsula (Hong et al., 2017).

The instantaneous seismic velocity changes in the lower crust of the Korean Peninsula were found to be −4.07% (±0.34% in the 95% confidence interval) to −0.73% (±0.11% in the 95% confidence interval) at frequencies of 0.03–0.08 Hz along the direction to the epicenter after the 2011 Tohoku-Oki megathrust earthquake (Hong et al., 2017). The Poisson's ratio changes for the seismic velocity changes were −2.78% (−3.07% $\leq \Delta\nu \leq$ −2.49% in the 95% confidence interval) to −0.38% (−0.45% $\leq \Delta\nu \leq$ −0.32% in the 95% confidence interval) according to an empirical relationship (Brocher, 2005; Vinh & Malischewsky, 2007).

Acknowledgments
The analyses conducted in this study are based on the earthquake source information and phase arrival times that are available from the Japan Meteorological Agency earthquake catalog (http://www.data.jma.go.jp/svd/eqev/data/bulletin/deck_e.html). We thank Professor Keisuke Yoshida for the data of principal stress field. We are grateful to Lucy Flesch (Editor) and two anonymous reviewers for valuable review comments that improved the presentation of this manuscript. This work was supported by the Korea Meteorological Administration Research and Development Program under grant KMI2018-02910. Additionally, this research was partly supported by the Basic Science Research Program through the National Research Foundation of Korea (NRF), which is funded by the Ministry of Education (NRF-2017R1A6A1A07015374).

References

Anderson, D. L., Minster, B., & Cole, D. (1974). The effect of oriented cracks on seismic velocities. *Journal of Geophysical Research*, *79*, 4011–4015.

Asano, Y., Saito, T., Ito, Y., Shiomi, K., Hirose, H., Matsumoto, T., et al. (2011). Spatial distribution and focal mechanisms of aftershocks of the 2011 off the Pacific coast of Tohoku earthquake. *Earth, Planets and Space*, *63*, 669–673.

Baisch, S., & Bokelmann, G. H. R. (2001). Seismic waveform attributes before and after the Loma Prieta earthquake: Scattering change near the earthquake and temporal recovery. *Journal of Geophysical Research*, *106*(B8), 16,323–16,337.

Bevington, P. R., & Robinson, D. K. (2003). *Data reduction and error analysis for the physical sciences* (pp. 320). New York: McGraw-Hill.

Brantut, N. (2015). Time-dependent recovery of microcrack damage and seismic wave speeds in deformed limestone. *Journal of Geophysical Research: Solid Earth*, *120*, 8088–8109. https://doi.org/10.1002/2015JB012324

Brenguier, F., Campillo, M., Hadziioannou, C., Shapiro, N. M., Nadeau, R. M., & Larose, E. (2008). Postseismic relaxation along the San Andreas Fault at Parkfield from continuous seismological observations. *Science*, *321*, 1478–1481.

Brenguier, F., Campillo, M., Takeda, T., Aoki, Y., Shapiro, N. M., Briand, X., et al. (2014). Mapping pressurized volcanic fluids from induced crustal seismic velocity drops. *Science*, *345*, 80–82.

Brocher, T. M. (2005). Empirical relations between elastic wavespeeds and density in the Earth's crust. *Bulletin of the Seismological Society of America*, *95*(6), 2081–2092.

Brown, E. T., & Hoek, E. (1978). Trends in relationships between measured in-situ stresses and depth. *International Journal of Rock Mechanics and Mining Science*, *15*(4), 211–215.

Brudy, M., Zoback, M. D., Fuchs, K., Rummel, F., & Baumgärtner, J. (1997). Estimation of the complete stress tensor to 8 km depth in the KTB scientific drill holes: Implications for crustal strength. *Journal of Geophysical Research*, *102*(B8), 18,453–18,475.

Cao, A., & Gao, S. S. (2002). Temporal variation of seismic b-values beneath northeastern Japan island arc. *Geophysical Research Letters*, *29*(9), 1334. https://doi.org/10.1029/2001GL013775

Cao, S., & Greenhalgh, S. (1995). Relative-error-based non-linear inversion: Application to seismic traveltime tomography. *Geophysical Journal International*, *121*(3), 684–694.

Carpenter, P. J., & Cash, D. J. (1988). Poisson's ratio in the Valles caldera and Rio Grande rift of northern New Mexico. *Bulletin of the Seismological Society of America*, *78*(5), 1826–1829.

Chaves, E. J., & Schwartz, S. Y. (2016). Monitoring transient changes within overpressured regions of subduction zones using ambient seismic noise. *Science Advances*, *2*(1), e1501289. https://doi.org/10.1126/sciadv.1501289

Christensen, N. I. (1996). Poisson's ratio and crustal seismology. *Journal of Geophysical Research*, *101*, 3139–3156.

Crampin, S. (1990). Alignment of near-surface inclusions and appropriate crack geometries for geothermal hot-dry-rock experiments. *Geophysical Prospecting*, *38*(6), 621–631.

Crampin, S., & Chastin, S. (2003). A review of shear wave splitting in the crack-critical crust. *Geophysical Journal International*, *155*, 221–240.

Crampin, S., & Zatsepin, S. V. (1995). Production seismology: The use of shear waves to monitor and mode production in a poro-reactive and interactive reservoir. *In 65th Ann. Int. SEG Meeting, Expanded Abstracts* (pp. 199–202). Houston, TX.

Efron, B., & Tibshirani, R. (1991). Statistical data analysis in the computer age. *Science*, *253*, 390–395.

Fortin, J., Guéguen, Y., & Schubnel, A. (2007). Effects of pore collapse and grain crushing on ultrasonic velocities and v_P/v_S. *Journal of Geophysical Research*, *112*, B08207. https://doi.org/10.1029/2005JB004005

Gonzalez-Huizar, H., Velasco, A. A., Peng, Z., & Castro, R. (2012). Remote triggered seismicity caused by the 2011, M9.0 Tohoku, Japan earthquake. *Geophysical Research Letters*, *39*, L10302. https://doi.org/10.1029/2012GL051015

Haimson, B. C., & Chang, C. (2002). True triaxial strength of the KTB amphibolite under borehole wall conditions and its use to estimate the maximum horizontal in situ stress. *Journal of Geophysical Research*, *107*(B10), 2257. https://doi.org/10.1029/2001JB000647

Hasegawa, A., Yoshida, K., Asano, Y., Okada, T., Iinuma, T., & Ito, Y. (2012). Change in stress field after the 2011 great Tohoku-Oki earthquakes. *Earth and Planetary Science Letters*, *355-356*, 231–243.

Hirose, F., Miyaoka, K., Hayashimoto, N., Yamazaki, T., & Nakamura, M. (2011). Outline of the 2011 off the Pacific coast of Tohoku earthquake (m_W 9.0)-seismicity: Foreshocks, mainshock, aftershocks, and induced activity. *Earth, Planets and Space*, *63*, 513–518.

Hong, T.-K., Lee, J., Chi, D., & Park, S. (2017). Seismic velocity changes in the backarc continental crust after the 2011 m_W 9.0 Tohoku-Oki megathrust earthquake. *Geophysical Research Letters*, *44*, 10,997–11,003. https://doi.org/10.1002/2017GL075447

Hong, T.-K., Lee, J., & Houng, S. E. (2015). Long-term evolution of intraplate seismicity in stress shadows after a megathrust. *Physics of the Earth and Planetary Interiors*, *245*, 59–70.

Hong, T.-K., & Menke, W. (2008). Imaging laterally varying regional heterogeneities from seismic coda using a source-array analysis. *Physics of the Earth and Planetary Interiors*, *166*, 188–202.

Hoshiba, M., Iwakiri, K., Hayashimoto, N., Shimoyama, T., Hirano, K., Yamada, Y., et al. (2011). Outline of the 2011 off the Pacific coast of Tohoku earthquake (m_W 9.0)—Earthquake early warning and observed seismic intensity. *Earth, Planets and Space*, *63*(7), 547–551.

Houng, S. E., Lee, J., & Hong, T.-K. (2016). Dynamic seismic response of a stable intraplate region to a megathrust earthquake. *Tectonophysics*, *689*, 67–78.

Iidaka, T., Muto, J., Obara, K., Igarashi, T., & Shibazaki, B. (2014). Trench-parallel crustal anisotropy along the trench in the fore-arc region of Japan. *Geophysical Research Letters*, *41*, 1957–1963. https://doi.org/10.1002/2013GL058359

Iidaka, T., & Obara, K. (2013). Shear-wave splitting in a region with newly-activated seismicity after the 2011 Tohoku earthquake. *Earth, Planets and Space*, *65*(9), 1059–1064.

Ikeda, T., & Tsuji, T. (2014). Azimuthal anisotropy of Rayleigh waves in the crust in southern Tohoku area, Japan. *Journal of Geophysical Research: Solid Earth*, *119*, 8964–8975. https://doi.org/10.1002/2014JB011567

Ikuta, R., Yamaoka, K., Miyakawa, K., Kunitomo, T., & Kumazawa, M. (2002). Continuous monitoring of propagation velocity of seismic waves using ACROSS. *Geophysical Research Letters*, *29*(13), 1627. https://doi.org/10.1029/2001GL013974

Imanishi, K., Ando, R., & Kuwahara, Y. (2012). Unusual shallow normal-faulting earthquake sequence in compressional northeast Japan activated after the 2011 off the Pacific coast of Tohoku earthquake. *Geophysical Research Letters*, *39*, L09306. https://doi.org/10.1029/2012GL051491

Irikura, K., & Kurahashi, S. (2012). Strong ground motions during the 2011 Pacific coast off Tohoku, Japan earthquake. In *Proceedings of the International Symposium on Engineering Lessons Learned from the 2011 Great East Japan Earthquake* (pp. 9–20). Tokyo, Japan.

Jo, E., & Hong, T.-K. (2013). V_P/V_S ratios in the upper crust of the southern Korean Peninsula and their correlations with seismic and geophysical properties. *Journal of Asian Earth Sciences*, *66*, 204–214.

Kaneshima, S., Ando, M., & Kimura, S. (1988). Evidence from shear-wave splitting for the restriction of seismic anisotropy to the upper crust. *Nature*, *335*(6191), 627.

Kato, A., Sakai, S., & Obara, K. (2011). A normal-faulting seismic sequence triggered by the 2011 off the Pacific coast of Tohoku earthquake: Wholesale stress regime changes in the upper plate. *Earth, Planets and Space*, *63*, 745–748.

Keulen, N., Stünitz, H., & Heilbronner, R. (2008). Healing microstructures of experimental and natural fault gouge. *Journal of Geophysical Research*, *113*, B06205. https://doi.org/10.1029/2007JB005039

Kido, M., Osada, Y., Fujimoto, H., Hino, R., & Ito, Y. (2011). Trench-normal variation in observed seafloor displacements associated with the 2011 Tohoku-Oki earthquake. *Geophysical Research Letters*, *38*, L24303. https://doi.org/10.1029/2011GL050057

Lay, T., Ammon, C. J., Kanamori, H., Xue, L., & Kim, M. J. (2011). Possible large near-trench slip during the 2011 m_W 9.0 off the Pacific coast of Tohoku Earthquake. *Earth, Planets and Space*, *63*, 687–692.

Lee, J., & Hong, T.-K. (2014). Dynamic lithospheric response to megathrust and precursory seismicity features of megathrust. *Physics of the Earth and Planetary Interiors*, *234*, 35–45.

Lee, J., Hong, T.-K., & Chang, C. (2017). Crustal stress field perturbations in the continental margin around the Korean Peninsula and Japanese islands. *Tectonophysics*, *718*, 140–149.

Lees, J. M., & Crosson, R. S. (1989). Tomographic inversion for three-dimensional velocity structure at Mount St. Helens using earthquake data. *Journal of Geophysical Research*, *94*(B5), 5716–5728.

Lockner, D. A., Walsh, J. B., & Byerlee, J. D. (1977). Changes in seismic velocity and attenuation during deformation of granite. *Journal of Geophysical Research*, *82*(33), 5374–5378. https://doi.org/10.1029/JB082i033p05374

Matsumoto, Y., Ishikawa, M., Terabayashi, M., & Arima, M. (2010). Simultaneous measurements of compressional wave and shear wave velocities, Poisson's ratio, and v_P/v_S under deep crustal pressure and temperature conditions: Example of silicified pelitic schist from Ryoke Belt, Southwest Japan. *Island Arc*, *19*, 30–39.

Minato, S., Tsuji, T., Ohmi, S., & Matsuoka, T. (2012). Monitoring seismic velocity change caused by the 2011 Tohoku-oki earthquake using ambient noise records. *Geophysical Research Letters*, *39*, L09309. https://doi.org/10.1029/2012GL051405

Miyazawa, M. (2011). Propagation of an earthquake triggering front from the 2011 Tohoku-Oki earthquake. *Geophysical Research Letters*, *38*, L23307. https://doi.org/10.1029/2011GL049795

Nakahara, H. (2015). Auto correlation analysis of coda waves from local earthquakes for detecting temporal changes in shallow subsurface structures: The 2011 Tohoku-Oki, Japan earthquake. *Pure and Applied Geophysics*, *172*(2), 213–224.

Nakajima, J., Matsuzawa, T., Hasegawa, A., & Zhao, D. (2001). Three-dimensional structure of v_P, v_S, and v_P/v_S beneath northeastern Japan: Implications for arc magmatism and fluids. *Journal of Geophysical Research*, *106*(B10), 21,843–21,857.

Nakata, N., & Snieder, R. (2011). Near-surface weakening in Japan after the 2011 Tohoku-Oki earthquake. *Geophysical Research Letters*, *38*, L17302. https://doi.org/10.1029/2011GL048800

Nakata, N., & Snieder, R. (2012). Time-lapse change in anisotropy in Japan's near surface after the 2011 Tohoku-Oki earthquake. *Geophysical Research Letters*, *39*, L11313. https://doi.org/10.1029/2012GL051979

Nur, A. (1972). Dilatancy, pore fluids, and premonitory variations of t_s/t_p travel times. *Bulletin of the Seismological Society of America*, *62*(5), 1217–1222.

Okada, T., Matsuzawa, T., Umino, N., Yoshida, K., Hasegawa, A., Takahashi, H., et al. (2015). Hypocenter migration and crustal seismic velocity distribution observed for the inland earthquake swarms induced by the 2011 Tohoku-oki earthquake in NE Japan: Implications for crustal fluid distribution and crustal permeability. *Geofluids*, *15*, 293–309.

Ozawa, T., & Fujita, E. (2013). Local deformations around volcanoes associated with the 2011 off the Pacific coast of Tohoku earthquake. *Journal of Geophysical Research: Solid Earth*, *118*, 390–405. https://doi.org/10.1029/2011JB009129

Ozawa, S., Nishimura, T., Suito, H., Kobayashi, T., Tobita, M., & Imakiire, T. (2011). Coseismic and postseismic slip of the 2011 magnitude-9 Tohoku-Oki earthquake. *Nature*, *475*, 373–376.

Peng, Z., Aiken, C., Kilb, D., Shelly, D. R., & Enescu, B. (2012). Listening to the 2011 magnitude 9.0 Tohoku-Oki, Japan, earthquake. *Seismological Research Letters*, *83*(2), 287–293. https://doi.org/10.1785/gssrl.83.2.287

Porritt, R. W., & Yoshioka, S. (2017). Evidence of dynamic crustal deformation in Tohoku, Japan, from time-varying receiver functions. *Tectonics*, *36*, 1934–1946. https://doi.org/10.1002/2016TC004413

Revenaugh, J., & Meyer, R. (1997). Seismic evidence of partial melt within a possibly ubiquitous low-velocity layer at the base of the mantle. *Science*, *277*, 670–673.

Sawazaki, K., & Snieder, R. (2013). Time-lapse changes of P-and S-wave velocities and shear wave splitting in the first year after the 2011 Tohoku earthquake, Japan: Shallow subsurface. *Geophysical Journal International*, *193*(1), 238–251.

Schubnel, A., Fortin, J., Burlini, L., & Guéguen, Y. (2005). Damage and recovery of calcite rocks deformed in the cataclastic regime. *Geological Society of London*, *245*, 203–221.

Shao, G., Li, X., Ji, C., & Maeda, T. (2011). Focal mechanism and slip history of 2011 m_W 9.1 off the Pacific coast of Tohoku earthquake, constrained with teleseismic body and surface waves, Earth. *Planets and Space*, *63*, 559–564. https://doi.org/10.5047/eps.2011.06.028

Shearer, P. M. (1988). Cracked media, Poisson's ratio and the structure of the upper oceanic crust. *Geophysical Journal International*, *92*(2), 357–362.

Shimojo, K., Enescu, B., Yagi, Y., & Takeda, T. (2014). Fluid-driven seismicity activation in northern Nagano region after the 2011 M9.0 Tohoku-oki earthquake. *Geophysical Research Letters*, *41*, 7524–7531. https://doi.org/10.1002/2014GL061763

Silverii, F., Cheloni, D., D'Agostino, N., Selvaggi, G., & Boschi, E. (2014). Post-seismic slip of the 2011 Tohoku-Oki earthquake from GPS observations: Implications for depth-dependent properties of subduction megathrusts. *Geophysical Journal International*, *198*, 580–596.

Simons, M., Minson, S. E., Sladen, A., Ortega, F., Jiang, J., Owen, S. E., et al. (2011). The 2011 magnitude 9.0 Tohoku-Oki earthquake: Mosaicking the megathrust from seconds to centuries. *Science*, *332*, 1421–1425. https://doi.org/10.1126/science.1206731

Sun, T., Wang, K., Iinuma, T., Hino, R., He, J., Fujimoto, H., et al. (2014). Prevalence of viscoelastic relaxation after the 2011 Tohoku-oki earthquake. *Nature*, *514*, 84–87. https://doi.org/10.1038/nature13778

Taira, T., Brenguier, F., & Kong, Q. (2015). Ambient noise-based monitoring of seismic velocity changes associated with the 2014 m_W 6.0 South Napa earthquake. *Geophysical Research Letters*, *42*, 6997–7004. https://doi.org/10.1002/2015GL065308

Takada, Y., & Fukushima, Y. (2013). Volcanic subsidence triggered by the 2011 Tohoku earthquake in Japan. *Nature Geoscience*, *6*(8), 637–641.

Takagi, R., & Okada, T. (2012). Temporal change in shear velocity and polarization anisotropy related to the 2011 M9.0 Tohoku-Oki earthquake examined using KiK-net vertical array data. *Geophysical Research Letters*, *39*, L09310. https://doi.org/10.1029/2012GL051342

Terakawa, T., Hashimoto, C., & Matsu'ura, M. (2013). Changes in seismic activity following the 2011 Tohoku-oki earthquake: Effects of pore fluid pressure. *Earth and Planetary Science Letters*, *365*, 17–24.

Tormann, T., Enescu, B., Woessner, J., & Wiemer, S. (2015). Randomness of megathrust earthquakes implied by rapid stress recovery after the Japan earthquake. *Nature Geoscience*, *8*, 152–158.

Vidale, J. E., & Li, Y. G. (2003). Damage to the shallow Landers fault from the nearby Hector Mine earthquake. *Nature*, *421*(6922), 524–526.

Vinh, P. C., & Malischewsky, P. G. (2007). An improved approximation of Bergmann's form for the Rayleigh wave velocity. *Ultrasonics*, *47*, 49–54.

Wadati, K. (1933). On the travel time of earthquake waves, II. *Geophysical Magazine*, *7*, 101–111.

Wang, X.-Q., Schubnel, A., Fortin, J., David, E. C., Guéguen, Y., & Ge, H.-K. (2012). High v_P/v_S ratio : Saturated cracks or anisotropy effects? *Geophysical Research Letters*, *39*, L11307. https://doi.org/10.1029/2012GL051742

Wiemer, S., & Wyss, M. (2000). Minimum magnitude of completeness in earthquake catalogs: Examples from Alaska, the western United States, and Japan. *Bulletin of the Seismological Society of America*, *90*(4), 859–869.

Xu, Z. J., & Song, X. (2009). Temporal changes of surface wave velocity associated with major Sumatra earthquakes from ambient noise correlation. *Proceedings of the National Academy of Sciences*, *106*, 14,207–14,212.

Yagi, Y., & Fukahata, Y. (2011). Rupture process of the 2011 Tohoku-Oki earthquake and absolute elastic strain release. *Geophysical Research Letters*, *38*, L19307. https://doi.org/10.1029/2011GL048701

Yamagiwa, S., Miyazaki, S., Hirahara, K., & Fukahata, Y. (2015). Afterslip and viscoelastic relaxation following the 2011 Tohoku-Oki earthquake (m_W9.0) inferred from inland GPS and seafloor GPS/acoustic data. *Geophysical Research Letters*, *42*, 66–73. https://doi.org/10.1002/2014GL061735

Yoshida, K., Hasegawa, A., Okada, T., Iinuma, T., Ito, Y., & Asano, Y. (2012). Stress before and after the 2011 great Tohoku-oki earthquake and induced earthquakes in inland areas of eastern Japan. *Geophysical Research Letters*, *39*, L03302. https://doi.org/10.1029/2011GL049729

Yukutake, Y., Honda, R., Harada, M., Aketagawa, T., Ito, H., & Yoshida, A. (2011). Remotely-triggered seismicity in the Hakone volcano following the 2011 off the Pacific coast of Tohoku Earthquake. *Earth, Planets and Space*, *63*, 737–740.

Zatsepin, S. V., & Crampin, S. (1997). Modelling the compliance of crustal rock—I. Response of shear-wave splitting to differential stress. *Geophysical Journal International*, *129*, 477–494.